Scientific African 19 (2023) e01501

Contents lists available at ScienceDirect

Scientific African

journal homepage: www.elsevier.com/locate/sciaf

A systematic study of the effect of graphene oxide and reduced graphene oxide on the thermal degradation behavior of acrylonitrile-butadiene rubber in air and nitrogen media

Bismark Mensah[a,*], David Sasu Konadu[a], Frank Nsaful[b], Prosper Naah Angnunavuri[c], Samuel Kwofie[d]

[a] Department of Materials Science and Engineering, CBAS, University of Ghana, Legon, Ghana
[b] Department of Food Processing and Engineering, CBAS, University of Ghana, Legon, Ghana
[c] School of Engineering, Department of Civil and Environmental Engineering, University of Energy and Natural Resources, Sunyani, Ghana
[d] Ghana Gas Company limited

ARTICLE INFO

Article history:
Received 14 October 2022
Revised 8 December 2022
Accepted 10 December 2022

Editor DR B Gyampoh

Keywords:
Acrylonitrile-butadiene rubber
Graphene and derivative graphene sheets (GDS)
G graphene oxide (GO) and reduced graphene Oxide (G)
Thermal degradation
Maximum degradation temperatures
Thermal degradation kinetics

ABSTRACT

Thermal degradation of acrylonitrile-butadiene rubber (NBR)-graphene oxide (GO)/reduced graphene Oxide (G) composites (NBR-GO/G) was studied in air O_2(g) and nitrogen N_2(g) media at ~800°C, using Thermal Gravimetric Analysis (TGA/DTG). The char yield of the composites was high the in N_2(g) medium. This was associated with lower weight loss (%) and higher maximum degradation temperatures, T_{max}(°C). Doyle simple kinetic approach was used for the first time to estimate the degradation kinetics of the NBR-GO/G composites and large amounts of activation energy E_a (KJ/mol) was observed, particularly for the NBR-GO composites. In O_2(g) medium, severe degradation of NBR occurred irrespective of the GO/G-filler content. This suggested that insignificant char yield was produced to protect the scission of the NBR backbone, as decomposition of the main chain seemed to have been accelerated by the high oxygenated moieties (C–O–C, –O–C=O and O–H) decorating GO/G-sheets. For instance, NBR showed ~89, ~21 and ~86 % weight residue, W_r (%) than $G_{0.1}$, $G_{0.5}$ and G_1 respectively and ~154, ~350, ~92 % higher than the respective $GO_{0.1}$, $GO_{0.5}$ and GO_1 samples. Although, NBR-G recorded higher W_r(%) than NBR-GO, NBR-GO generally slowed the degradation of NBR than NBR-G composites, possibly due to the presence of high concentration of interactions (NBR—S_x—GO—S—NBR and NBR—O—$H^{\sigma+}$—N $^{\sigma-}$—C—NBR) which raised the E_a (KJ/mol) barrier for decomposition. The high thermal stability and compression set (%) properties of NBR-GO/G composites obtained as compared to pure NBR indicated that solution processing techniques used in this current work was very effective than those compounded with melt mixing methods or with GO/G-functionalized nanoparticles. Therefore, this present study provides insights on tailoring rubber-graphene based materials for thermally harsh and high pressure applications such as; oil/gas drilling hose, oil/gas seals, gasket and tire tread materials.

* Corresponding author.
E-mail address: bismarkmensah@ug.edu.gh (B. Mensah).

https://doi.org/10.1016/j.sciaf.2022.e01501

Introduction

The viscoelastic nature of rubbers render them as promising materials in the polymer industry for various applications including high deformation (flexible/stretchable) sensors [1–6], structural materials [7–9], flame retardants [10,11] and thermal insulating materials [12–14]. The long-term usages with safety guarantee for applications in high temperature environments are mostly focused on the development of synergy systems, comprising of the rubber matrix and desired content of reinforcements like; metal oxides [14], nanoclays [15–17], carbon nanotubes [18,19], boron nitride nanotubes [20] and carbon blacks [21,22]. Successful tailor-made elastomeric-filler composite products are able to delay the rapid thermal degradation of the bulk matrix due to successful dispersions of the fillers and the strong matrix-filler interactions [20,23-25].

The emergence of graphene and derivative graphene sheets (GDS) has already created a tremendous revolution in rubber-Nano-Technology [26–28]. This is due to the unique properties of the GDS, which include; high Young's modulus of ~1 TPa, excellent mechanical strength, high thermal conductivity of ~5000 W/(m·K) and unparalleled electrical conductivity of ~6000 S/cm [29,30]. By careful engineering, GDS can transfer some of these unique properties to the almost useless virgin elastomeric matrix [26–28]. A lot of work on elastomer-GDS composites research has been reported with several property enhancements [7,26,27]. Greater portion of these studies have focused more on curing [31–33], reinforcement/mechanical strength [28,34-36], barrier properties [8,37,38], thermal conductivity [28,39-41] with few studies on thermal degradation behaviors [25,41].

On thermal degradation studies, thermal gravimetric analysis (TGA) and the derivative thermal gravimetric analysis (DTG) have been widely used to estimate the thermal decomposition of rubber-GDS-based systems. When Dong et al. [25] reinforced natural rubber (NR) with only 1.1 part per hundred of rubber (phr) graphene, the weight residue (%) derived from the TGA curves for the NR-graphene was higher than that of pure NR. Other studies have focused on improving the thermal degradation resistance of elastomers by functionalization of the GDS before incorporating them into the matrix [26,28]. For example, Xiong et al. [41] functionalized graphene oxide (GO) with ionic liquid and incorporated it into bromo-isobutylene isoprene rubber (BIIR), an enhancement in thermal degradation resistances were observed as compared to the pure BIIR. Also, improvement in thermal degradation stability of carboxylated acrylonitrile-butadiene rubber (NBR)-GO composites was observed by Manna et al. [42] after functionalization of GO with hexadecyl amine (HDA).

Moreover, it has been observed that the majority of thermal decomposition studies of rubber-GDS composites were done in N_2(g) medium and the kinetic energies of decomposition were calculated based on Ozawa and Kissinger et al. [43–45] approaches. Although, thermal stability of silicone rubber in only air O_2(g) medium was recently reported by Wang et al. [35]. It was observed that thermal degradation behavior of the composites depended greatly on size effect, that is, the middle-size G obtained the best compared to the small or large-sized GO and G.

Furthermore, Mensah et al. [46] earlier conducted a study on the curing, tensile and thermal stability (in N_2(g) medium) behavior of NBR-GO composites. It was observed that increasing GO content improved the tensile properties and shielded the NBR matrix from further decomposition. Thus, it can clearly be ascertained that the thermal degradation behavior of rubber-GDS based systems may be dependent on several factors including; type of GDS, chemistry of GDS, thermal conductivity, particle size, dispersions of the GDS, the characteristics of the matrix used as well as the medium in which the thermal degradation study was carried [28,39-41].

Therefore, with these shortfalls in rubber-GDS research and together with global demand of multifunctional of materials, further works on the thermal degradation behavior of rubber reinforced with different rubber matrix and GDS types, particularly in different decomposition environments like nitrogen, N_2(g) and air O_2(g) media etc., are worth exploring. In this present work, we prepare a composite of NBR reinforced with GO and G-nanosheets and investigate the curing, network density and compression set, CS (%) properties. The thermal degradation kinetics of the NBR-GO/G composites were studied separately in N_2(g) and air O_2(g) media by using TGA/DTG and Doyle method [47,48]. The results obtained provide insights on the need to select and design appropriate rubber matrix and GDS for thermally harsh and high pressure environments.

Experimental

Materials

The base rubber matrix used is acrylonitrile-butadiene rubber (NBR) with the trade name KNB 25LM^{TM}, and acrylonitrile content (ACN) of 20-30%. The NBR was supplied by the Kumho Petrochemical Company, Korea. The vulcanization ingredients; zinc oxide (ZnO), stearic acid (SA), sulfur (S), and N-cyclohexile 2-benzotiazole sulfonamide (CZ) were all obtained from Intelligent Polymer Nano Lab (IPNL), Polymer Nano-technology Department, Jeonbuk National University, South Korea. The graphene oxide (GO) was synthesized from natural graphite (GRT) powder by using the modified Hummer's method [49,50], where GRT was oxidized and later exfoliated by ultra-sonication. Some amount of the GO was weighed and reduced into reduced graphene oxide (G), which is close to pristine graphene [26,50]. The reduction was done by using desired amount of hydrazine (N_2H_4) and NH_4OH. The detailed synthesis method for the production of GO and G and characterizations done on GO and G were reported earlier by Mensah et al.[50].

Sample design and preparation

The compound formulation expressed as parts per hundred of rubber (phr) with their corresponding codes are presented in Table I. The preparation of the NBR, and NBR-GO/G-composites nanocomposite was effectively attained by combined method of solution mixing and open two-roll milling [46,51]. Briefly, the NBR was cut into pieces and dissolved in solvent (acetone) under 60 °C temperatures for ~12 h.

The GO and G were separately dispersed homogeneously in dimethylfuran (DMF) by prolonged ultrasonication for ~2.5 h, in order to separate the sheets from each other. The solutions of GO/DMF and G/DMF were each mixed with NBR/acetone mixture separately. The mixtures were then stirred vigorously on a magnetic stirrer at ~60 °C for ~12 h until a homogenous mixture of the composition was obtained. To avoid phase separation between the matrix and the GO/G-sheets, de-ionized water was added to the homogeneous mixture while still stirring. The resulting composites (NBR-GO and NBR-G) were oven dried at ~80 °C for about ~6 h, so as to eliminate entrapped liquid from the mixtures. Using a two-roll mill (Farrel 8422, USA), the curing materials (ZnO, SA, CZ, and S) were gradually added one by one and combined to obtain solid masses. The homogeneously milled samples were sheeted out and allowed to cool overnight. The various formulations were cured in a metallic square mold of dimension (15 cm x 15 cm) with ~0.1 cm thickness in-between Mylar film, using a hot press machine (Caver WMV50H, USA), at the optimum cure conditions. A pressure of ~11 MPa and a temperature of 160 °C were used as optimum cure conditions in the hot-pressing process. After allowing the cured samples to cool overnight, they were cut into standard shapes for further analysis and characterizations.

Characterization

Vulcanization properties

The curing properties of the various compounds; NBR and NBR-GO/G composites, were investigated using an oscillating die cure rheometer (ODR) machine procured from IPNL, JBNU, South Korea, to identify the optimum cure time at 160 °C using about ~9-10 g of each sample. The various curing parameters of the various compounds were acquired from the rheo-curves, analyzed, and reported. The properties include; maximum torque (M_H), minimum torque (M_L), change in torque ($\Delta M = M_H - M_L$), onset of cure time (t_{s2}), optimal cure time (t_{90}), and curing rate index ($CRI = 100/(t_{90}-t_{s2})$).

Scanning electron microscopy (SEM)

The morphologies of the GO and G powders, NBR, and NBR-GO/G composites were observed by using SEM technique. The composites were first cryogenically fractured before being sputter-coated with platinum to increase their electrical conductivity at the observing surfaces. Field emission SEM/energy dispersive x-ray spectroscopy (EDS) (JEOL, JSM 599, Japan) was used to examine the surface morphologies including identification of elements in the various materials. The test was achieved within ~40 min.

Transmission electron microscopy (TEM)

Ultrathin specimen (thinner than 100 nm) for TEM observation were cryogenically cut with a diamond knife using an ultrathin microtome (UCT, Leica Ultracut, EMFC7) and collected on 200-mesh copper grids. A transmission electron microscope was used to observe the exfoliation of GO and G-sheet nanosheets in NBR rubber (TEM, JEOL, JEM2100). The TEM machine was used to observe exfoliated DMF/GO and DMF/G solutions that were dropped on the mesh separately.

Crosslinking density by equilibrium swelling test

By equilibrating the produced samples in methyl-ethyl ketone (MEK) (molar volume of 89.6 mL/mol) for ~72 hours at room temperature, the equilibrium swelling of the vulcanized NBR and NBR-GO/NBR-G composites was evaluated. The degree of swelling (Q_r) was calculated using the absorbed amount of MEK (W_s-W_i) and the dried weight (W_{dr}) of samples by using Eq. (1).

$$Q_r = (W_s - W_i)/W_{dr} \tag{1}$$

where, W_i and W_s are the initial and final weights of (NBR, NBR-GO and NBR-G) before and after swelling. The cross-linking density N_c (mol/cm^3) of the vulcanizates was calculated by using Flory–Rehner model [52] in Eq. (2).

$$n_c = -[\ln(1 - v_2) + v_2 + \chi_1 v_2^2]/v_1(v_2^{1/3} - v_2/2) \tag{2}$$

where, v_2 is the volume fraction of polymer in swollen gel at equilibrium, which is given as $1/Q_r$. The v_1 is a molar volume of swelling media (MEK). The interaction parameter (χ_1) between MEK and NBR was calculated to be 0.384, where the solubility parameters (δ) of NBR (δ_p) and MEK (δ_s) was 8.9 cal$^{1/2}$/cm$^{-3/2}$ and 9.27 cal$^{1/2}$/cm$^{-3/2}$ respectively, by using Bristow–Watson [53] Eq. (3);

$$\chi_1 = \beta_1 + (v_1/RT)(\delta_s - \delta_p)^2 \tag{3}$$

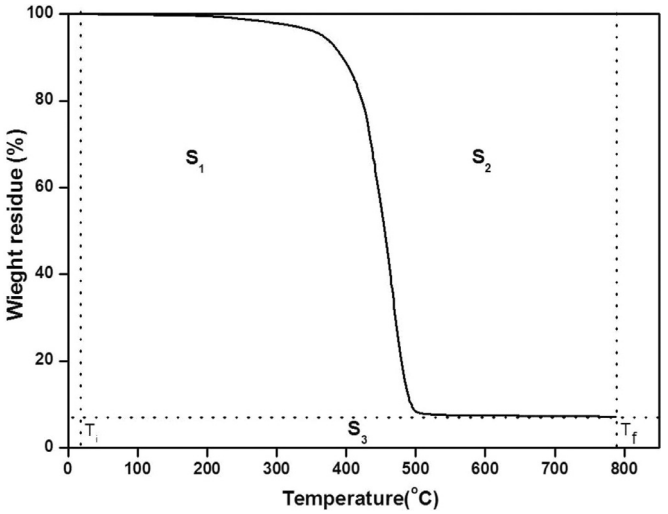

Fig. 1. TGA curves based on integral procedural degradation temperature (IPDT) approach.

where, R, T, and β_1, are universal gas constant (8.314 J/mol K), absolute temperature, and lattice constant (usually about 0.34).

Compression set properties

The compression set CS (%) of the vulcanized NBR and NBR-GO/G composites were determined according to ASTM D 395, same with the approach earlier reported by GS et al. [54] by using cylindrical specimens (~12.5 mm height and ~29 mm diameter) and by applying a 25 % compression. Initially, the samples average heights were measured using caliper and were then kept in an air oven at the testing temperatures of 25, 50, 100 and 200 °C respectively, each for 72 h. The samples were later taken out of the oven and allowed to cool at room temperature for ~30 min. The final height was then measured and the compression set CS (%) was calculated using the Eq. (4);

$$CS(\%) = (H_o - H_f)/(H_o - H_s) \tag{4}$$

where H_o and H_f are the initial and final height of the specimen and H_s (~9.5 mm) is the height of the spacer bar used.

Thermal degradation and kinetics study

DSC-TGA (TA Instrument, SDT Q600 V20.9 Build 20, USA) was used to study the thermal degradation behavior of the GO/G-sheets, and their compounds with NBR. The conditions were nitrogen and oxygen atmosphere, equilibrium temperature of ~30 °C and heating rate of 10 °C/min to a maximum temperature of ~800 °C. The thermal stability behavior of NBR and NBR-GO/G-composites were studied based on the maximum degradation temperature (T_{max}) from the derivative thermograph (DTG), weight residue (%) from the TGA curves, initial degradation temperature (IDT) and final degradation temperature (FDT). Later, the Doyle approach [47,48], where the integral procedural degradation temperature (IPDT) which correlates with the volatile parts of the polymeric materials, and widely used to evaluate the overall inherent thermal stability of polymeric materials in the degradation process, was also adopted for the first time in this present work to study the thermal degradation kinetics behavior of NBR-GO/G composites in air and nitrogen media. The IPDT is usually estimated from the TGA curves using the following Eq. (5-7), where A^* is the area ratio of the total area of the experimental curve divided by the total TGA curve, $K^*$is the coefficient, T_i is the initial experimental temperature (~30°C in this study), and T_f is the final experimental temperature (~800°C). S_1, S_2, and S_3 are the areas of the three regions into which the TGA plot had been divided, as shown in Fig. 1 below.

$$\boldsymbol{IPDT = A^* K^* \left(T_f - T_i\right) + T_i} \tag{5}$$

$$\mathbf{A^*} = \frac{(\mathbf{S_1} + \mathbf{S_2})}{(\mathbf{S_1} + \mathbf{S_2} + \mathbf{S_3})} \tag{6}$$

$$\mathbf{K^*} = \frac{(\mathbf{S_1} + \mathbf{S_2})}{(\mathbf{S_1})} \tag{7}$$

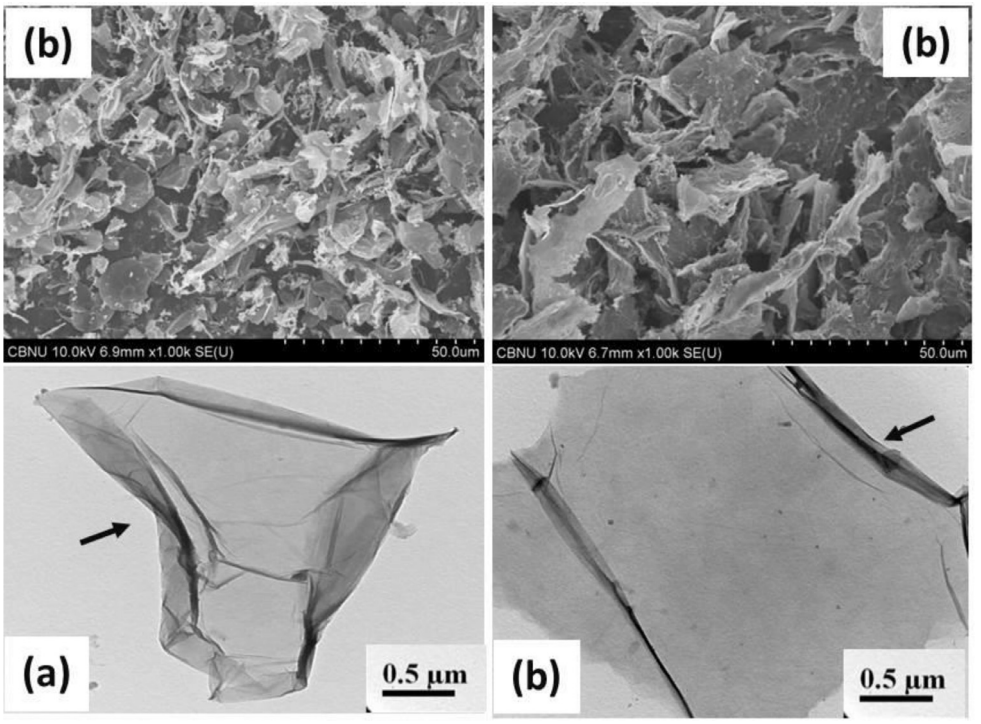

Fig. 2. SEM analysis of (a) GO-sheets and (b) G-sheets (c) TEM image of GO-sheets and (d) TEM image of G-sheets.

Results and discussions

Characterization of GO/G sheets: structure and morphology

The SEM morphology of GO and G-sheets are clearly presented in Fig. 2(a) and Fig. 2 (b), respectively. Layered crystalline formations exist in graphite (interlayer spacing of ~0.34 nm) [55–58]. In comparison to G-sheets (Fig. 2b), Fig. 2a shows that when graphite is oxidized and exfoliated into GO sheets, evidence of some of the sheets appearing to be severely corrugated or deformed are seen.

The G-sheets seems to be relatively solid, with minimal wrinkling effects and exhibiting tendencies of the presence of crystalline impurities. Based on the SEM scale, the average thickness of the GO/G sheets was estimated to be ~0.5-4 nm. The wrinkling and corrugating structures of GO is shown in the TEM image (Fig. 2c) while the restoration of the wrinkled structure of GO into G-sheets was achieved by using hydrazine (N_2H_4) and NH_4OH [49,59]. As seen in the TEM image in Fig. 2d, by using the given TEM scale bar, GO and G-sheets show an estimated average thickness of ~0.83-5 nm with hydrodynamic lengths of ~9-150 nm, measured by dynamic light scattering, as reported recently in the other work of Mensah et al. [60]. The structure and morphological features of GO/G-sheets in the SEM and TEM images are consistent with those earlier reported [26,58,61-63], which confirms GO/G-sheets as nanoparticles.

Thermal degradation behavior of GO/G-sheets

The Fig. 3 is the TGA curves for the powdered nanoparticles of GO and G. The initial T_{onset} (°C) and final T_{max} (°C) degradation temperatures were taken at 10 and 90 % weight loss (%) respectively. The T_{onset} (°C) of GO and G sheets were observed at ~93.4 and ~198.5°C respectively, while the T_{max} (°C) of GO and G was seen around ~796.4 and ~677 °C respectively. The initial degradation of GO and G may be ascribed to the evaporation of CO, CO_2 and water moisture from the sheets. The weight residue (%) of GO and G-sheets, after major decomposition at 800°C was ~48 % and ~70 % respectively. Thus, a higher temperature was required to decompose tight polar groups on GO-sheets, which consequently led to higher weight loss compared to G-sheets. The G-sheets although required lower temperature to be decomposed, yet in comparison to GO sheets, decomposition of G-sheets results in an increase in char yield, which delayed and protected the sheets from further breakdown. As earlier reported [32,51,64], the reduced oxygen concentration of G-sheets contributes to their thermal breakdown stability improvement. G-sheets have also been shown to possess better thermal stability than GO-sheets, owing to their capacity to recover from corrugating and wrinkling structures through the reduction process of GO [25,27,65]. Meanwhile, detailed characterization of these same fillers (GO and G-sheets) which include; UV-vis spectroscopy,

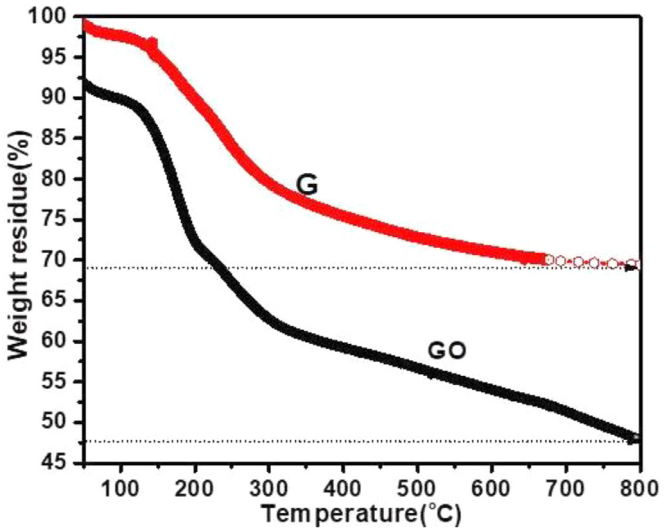

Fig. 3. TGA curves for GO and G-sheets

Raman spectroscopy, x-ray photoelectric spectroscopy (XPS) analysis, FT-IR etc. was reported by Mensah et al. [50] and all the properties observed for the GO and G-sheets were in accordance with those reported in literature [26,49,57,66-68].

Characterization of NBR-GO/G composites

Vulcanization behavior

The vulcanization properties which include; scorch time (t_{s2}), optimum cure time (t_{90}), minimum and maximum torque (M_L & M_H) and strength index ($\Delta M = M_H - M_L$) of NBR, loaded with variable amount (0.1∼1 phr) of GO and G fillers are plotted in Fig. 4 (a-d). In the presence of GO or G-sheets, the t_{s2} of the composites extended more than the pure NBR. The NBR-GO composites showed much longer t_{s2} than NBR-G systems. For processing stability and safety of the rubber and its final product, longer t_{s2} may be appreciable [26,32,69]. However, properties like the acidic nature of the GO/G-sheets, the chemistry of the GO/G sheets [26,27,32], the physical structure of the sheets (degree of wrinkling/corrugation of the sheets) [26,62,63,70], thermal properties [25,58,71] of the sheets, as well as the viscosity of the matrix, are all factors that may contribute to the extension of t_{s2} and t_{90} of rubber-GDS composites [26,32,69]. As the GO/G-sheets were incorporated into the NBR matrix, the cure rate index (CRI) of the composites was increased as compared to the gum (NBR). The NBR-G composites outperformed the NBR-GO systems.

In terms of polarity, the curing properties of NBR-GO/G were better than that of non-polar ethylene-propylene-diene monomer (EPDM) systems, owing to their unsaturated sites (ENB) of EPDM [60,72-74]. In addition, when GO/G was added to the NBR matrix, the rheological mechanical strength indices; viscosity (M_L), crosslink density (ΔM) and mechanical strength (M_H) of the composites were improved as compared to gum. This was supposed to be due to the creation of tighter network structures like; NBR–S_x–G–S–NBR or NBR–S_x–GO–S–NBR between the oxygen groups (C–O–C, –O–C=O and O–H) on the GO/G-sheets and the NBR matrix, as depicted in Fig. 5.

A physical interaction between the O−H of the GO/G-sheets and the nitrile group (−C≡N) of NBR through hydrogen bonding was previously observed [26,32]. Thus, the homogenous dispersions of the GO/G-sheets in the NBR matrix, and their interactions (physical and chemical), may influence the overall mechanical and thermal degradation properties of the related composites.

SEM/EDS analysis of NBR and NBR-GO/G composites

The SEM images of representative compounds; NBR, G_1 and GO_1 are shown in Fig. 6a, Fig. 6b and Fig. 6c respectively. It is usually difficult to see nano-sized particles such as carbon nanotubes and graphene sheets in rubber matrix, as they often embed themselves deeply in the matrix. Techniques was adopted by Nah et al. [75,76] by imposing forces on the composites that leads to migration of these nanoparticles from the rubber matrix to the observing surfaces. Although, no such stress was used in this present study, however when carefully observed, wrinkled-like GO/G sheets covered with NBR molecules and homogeneously distributed within the matrix, are seen at the observing surfaces of the composites. The pure matrix (Fig. 6a) did not show such observation; instead, cryogenically induced surface irregularities can be seen.

Wrinkled G-sheets covered with silicone rubber molecules was recently also reported by Wang et al.[35]. Such representative corrugated/wrinkling surface morphologies exhibited by GO/G-sheets are widely reported to be useful in mechanical interlocking of the matrix, leading to transfer of load at the interface of GO/G-matrices. This results in enhanced mechanical properties for the composites compared to the pure matrix [62,77,78].

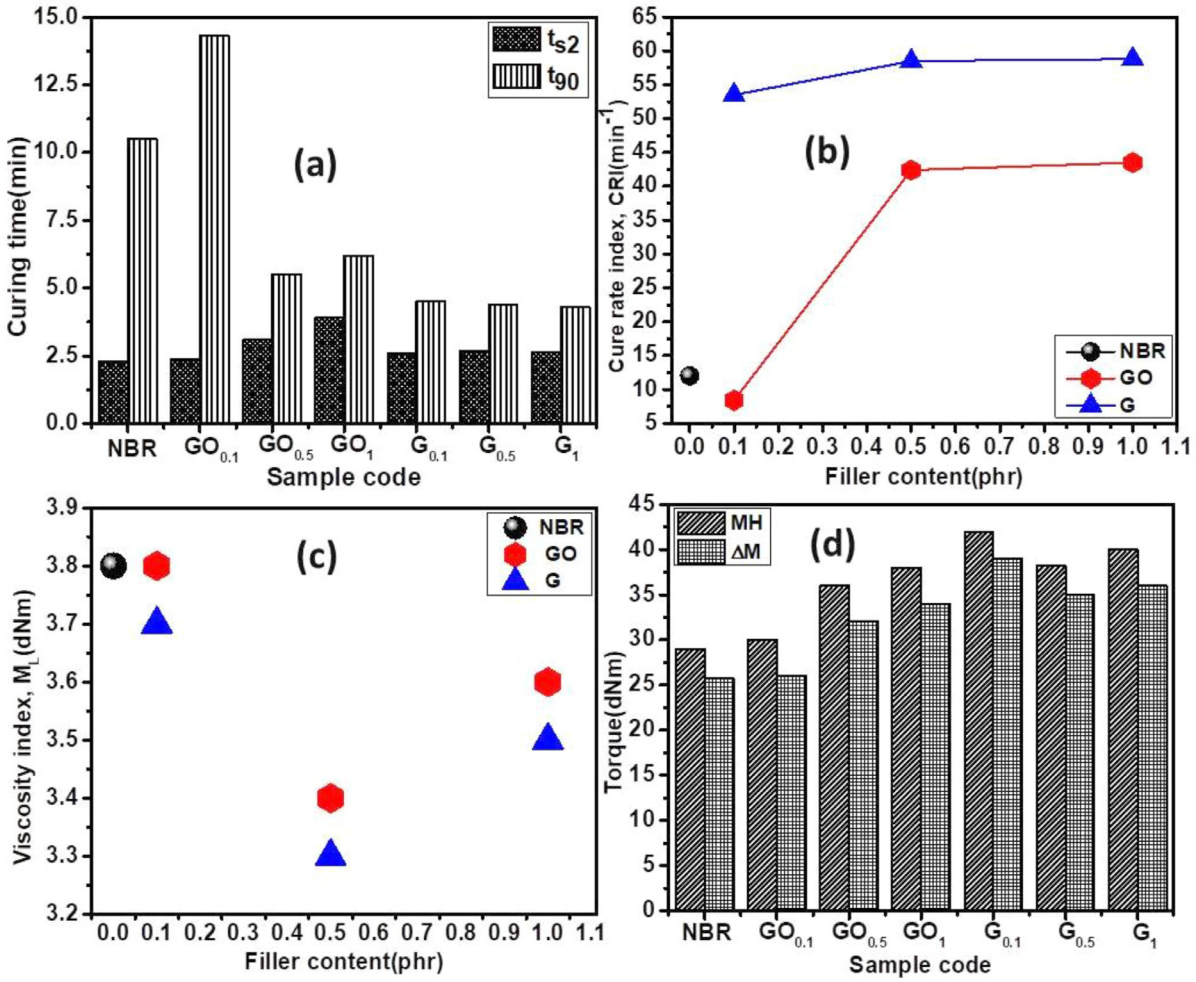

Fig. 4. Curing properties of NBR and NBR-GO/G composites; (a); scorch time (ts2), optimum cure time (t90) (b) effect of GO/G content versus CRI (min−1), (c) viscosity index (ML) and (d) crosslinking density (MH) and mechanical strength index (ΔM).

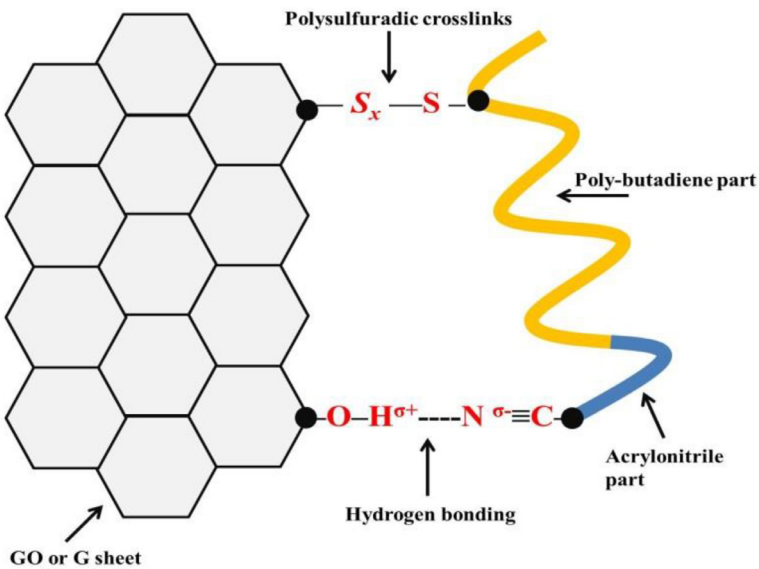

Fig. 5. Illustration of the interactions between NBR rubber chain, the GO or G-sheets, sulfur curative and the oxygen functionalities.

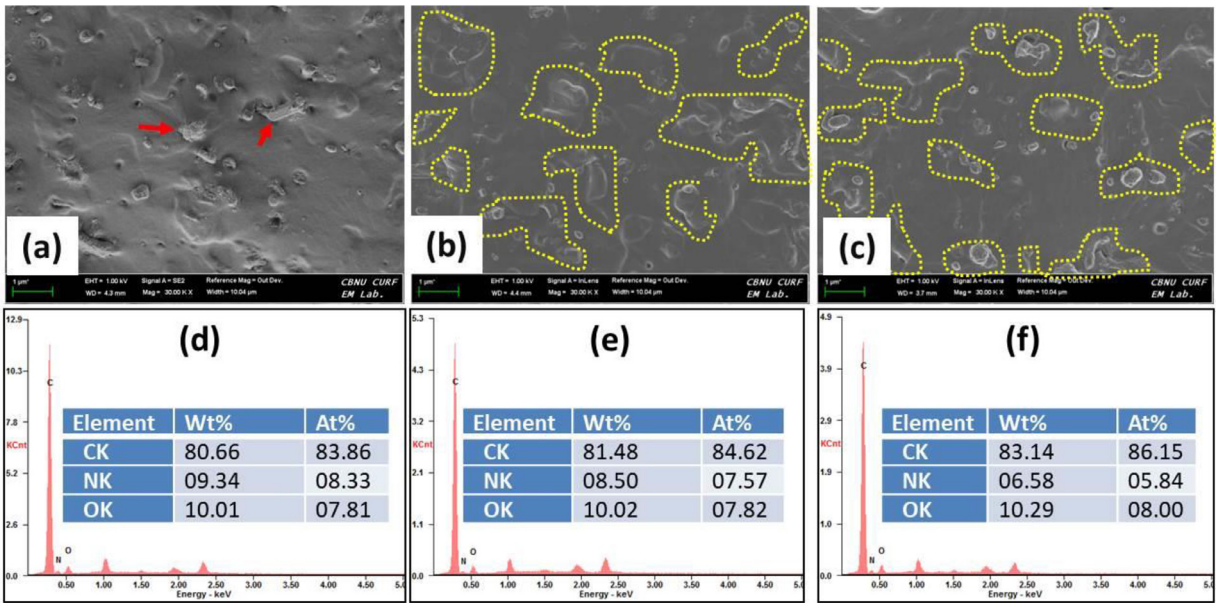

Fig. 6. SEM images of (a)NBR (b) NBR-G1 and (c)NBR-GO1. And the EDS analysis of (d) NBR (d) G1 and (c) GO1.

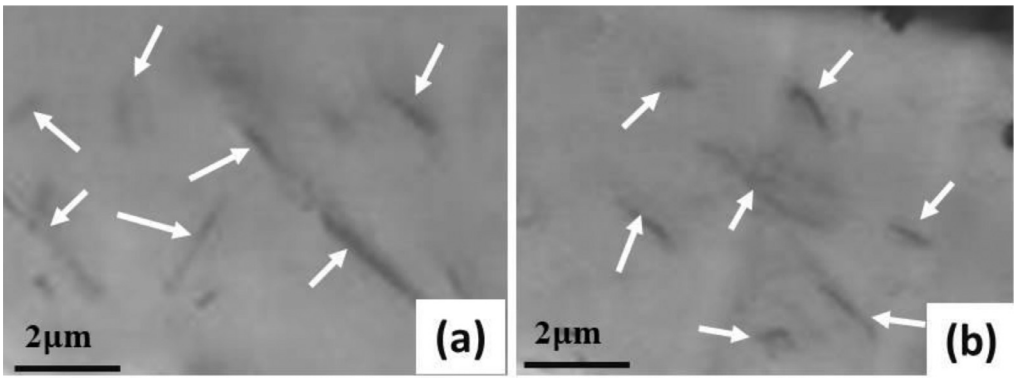

Fig. 7. TEM image of NBR loaded with 1 phr of (a) GO1 and (b) G1 sheets.

Earlier, FT-IR technique was used to examine the chemical functionalities of uncured and cured NBR-GO and NBR-G, including their blends with ethylene-propylene-diene monomer rubber (EPDM) [32,60]. Currently, EDS technique is adopted to qualitatively distinguish the prominent elements in NBR, NBR-GO and NBR-G compounds. The EDS of representative samples of NBR, G_1 and GO_1 are respectively presented in Fig. 6d, Fig. 6e and Fig. 6f. The prominent peaks coming from the elements oxygen (O), carbon (C) nitrogen (N) were used to identify the compounds. The order of reducing oxygen content is given by $GO_1 > G_1 >$ NBR, owing to numerous oxygen functionalities on the GO/G sheets. The nitrogen content increased by $GO_1 > G_1 >$ NBR; this trend was due to the presence of nitrile functions (−C≡N) in NBR [79,80]. That of the composites was found to be low, probably due to reactions of −C≡N groups with GO/G sheets. The reduction of GO into G by using hydrazine (N_2H_4) and NH_4OH [49] might be the reason for the high content of nitrogen content in G_1 than GO_1. These elements may come from groups that could play roles in crosslinking reactions and influence filler-polymer interactions and the overall thermal and physico-mechanical properties of the resulting compounds.

TEM analysis of NBR, NBR-GO/G composites

The TEM images of the NBR filled with 1phr of GO and G are shown in Fig. 7a and Fig. 7b respectively. Clearly, the GO/G-sheets seem to show homogeneous dispersions within the NBR matrix, indicating the effectiveness of solution mixing as a technique for reinforcing rubber matrices containing GO or G-sheets as summarized in the review reported Mensah et al. [26]. The sheets seem to exhibit coiling and corrugating nature coated with the rubber molecules [26,32,42]. Similar to those earlier observed in the SEM analysis, this effect improves the confinement of adjacent rubber chains for effective stress deflection at the interface [26,32,42].

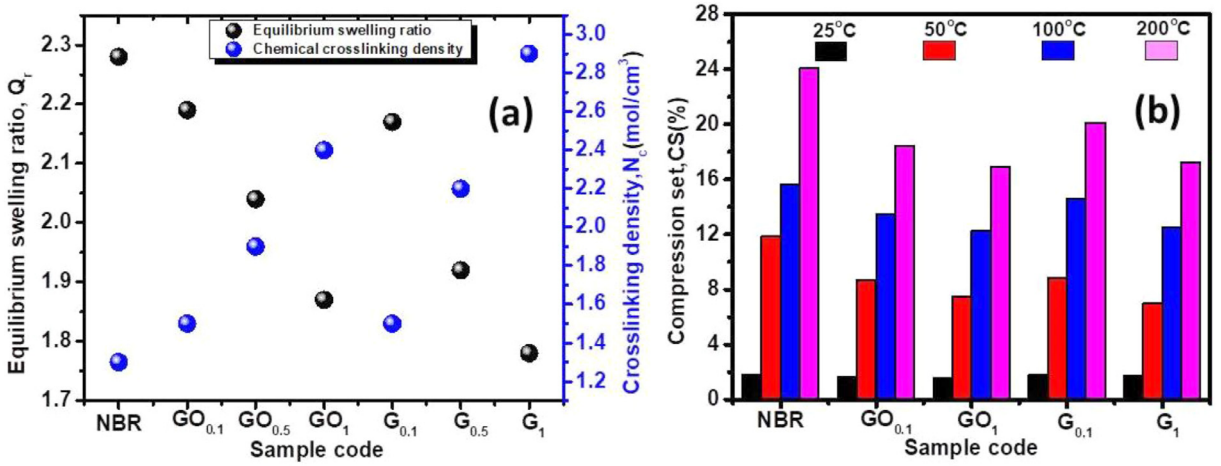

Fig. 8. Reinforcement and memory recovery ability of NBR-GO/G composites measured by (a) crosslinking density Nc(molcm−3) and (b) compression set CS (%).

Crosslinking density and compression set

The effect of loading of GO and G-sheets on the swelling ratio (Q_r) and the chemical crosslinking densities N_c(molcm^{-3}) of NBR matrix is shown in Fig. 8a The Q_r for NBR matrix was high, however, incorporating the fillers (GO/G-sheets) into NBR matrix resulted in decline of the Q_r properties. This was attributed to the reduction in molecular weight between crosslinks, which caused the network's free volume and solvent permeability to significantly decrease [54,69,81]. The low Q_r values for the composite may be ascribed to factors like; evenly distributions of the GO/G-sheets, their improved interactions with the NBR matrix (NBR−GO/G−S_x−NBR and NBR−GO/G−NBR) and interactions among themselves; filler-filler interactions (GO−GO, GO−S_x−S−GO, G−G or G−S_x−S−G) [26,32]. It can be suggested that; while the increase in N_c(molcm^{-3}) for the G-composites may be controlled by mere dispersions or increased amount of G−G or G−S_x−G bonds in NBR, that of the GO-sheets may mainly be due to desired dispersions as well as the strong interactions of GO-sheets with the NBR matrix, owing to the numerous active oxygenated moieties possessed by GO-sheets [26,49,60]. As a result, the low Q_r confirms the successful dispersion of the GO/G-sheets within the NBR matrix, which has the potential to improve the various physico-mechanical properties of the composites, as compared to the virgin matrix.

Also, the compression set CS (%) properties of the representative samples of NBR, $GO_{0.1}$, GO_1, $G_{0.1}$ and G_1 performed at temperatures of 25-200 °C are shown in Fig. 8b. The CS (%) values increased as filler content and temperature were increased respectively. In general, an increase in CS (%) indicates the elastomer/composite material's ability to recover memory that has been lost or deteriorated [82]. When compared to the gum, the composites have a lower CS (%), signifying a higher percentage increase in memory retainable behavior. The increased reinforcing effect of GO/G-sheets in NBR (physical presence, enhanced dispersions and strong bond with the matrix) may be responsible for the lower values of CS (%) behavior observed for the composites [26,50] in relation to the gum. These interactions, tighten the structures of the composites, disallowing the recovery of the bulk structure, after prolong thermal deformation. By comparison, the G-composites slightly showed higher CS (%) properties than the GO-composites counterpart, which is in accordance with the network density, N_c(molcm^{-3}). The CS (%) properties at room temperature of the present compounds (∼1.7-1.82 %) are comparable with that of NBR reinforced with (0-50 phr) silanized silica reported by Senthilvel et al.[82] and have outperformed that of NR-carbon black, NR-GO and NR-carbon nanotubes, whose CS (%) values were reported to be ∼3.5-4.6 %, by Zang et al. [83]. However, it must be noted that, at this high temperature conditions (100-200 °C) of sets, thermal degradation and recombination of crosslinks may be possible [54,69].

Thermal degradation of NBR-GO/G in nitrogen medium

The weight residue, W_r(%) as a function of temperature for NBR loaded at different concentrations (0.1-1 phr) of GO and G decomposed in nitrogen medium are presented in Fig. 9 (*a-c*) with magnified graphs inserted in each plot for clarity. The effect of GO or G-sheets loading on the W_r(%) of the compounds is also compared in Fig. 9d. It is generally observed that incorporation of the GO/G-sheets into NBR matrix delayed thermal decomposition of the NBR matrix in the nitrogen medium, which is very obvious at higher loading of the fillers. For example, at 0.1 phr, $GO_{0.1}$ and $G_{0.1}$ increased the W_r(%) of NBR more than 15 and 18% respectively, while the effect shot up to 29 and 63 % for the GO_1 and G_1 composites respectively.

Furthermore, the maximum temperature of degradation, T_{max} (°C) of the compositions at different GO/G loading is shown in Fig. 10 (a-d) while the effects of GO/G-sheets loading on T_{max} (°C) are compared in Fig. 10d. The T_{max} (°C) for the composites are generally higher than that of the pure matrix, at all filler loading levels. The combined effect of the physical presence of the GO/G-sheets, their enhanced dispersions and particularly their strong interactions with the NBR matrix, by creating numerous tighter networks (NBR−S_x-G−S−NBR, NBR−S_x−GO−S−NBR and O−H$^{\sigma+}$−N $^{\sigma-}$−C−) may be the main

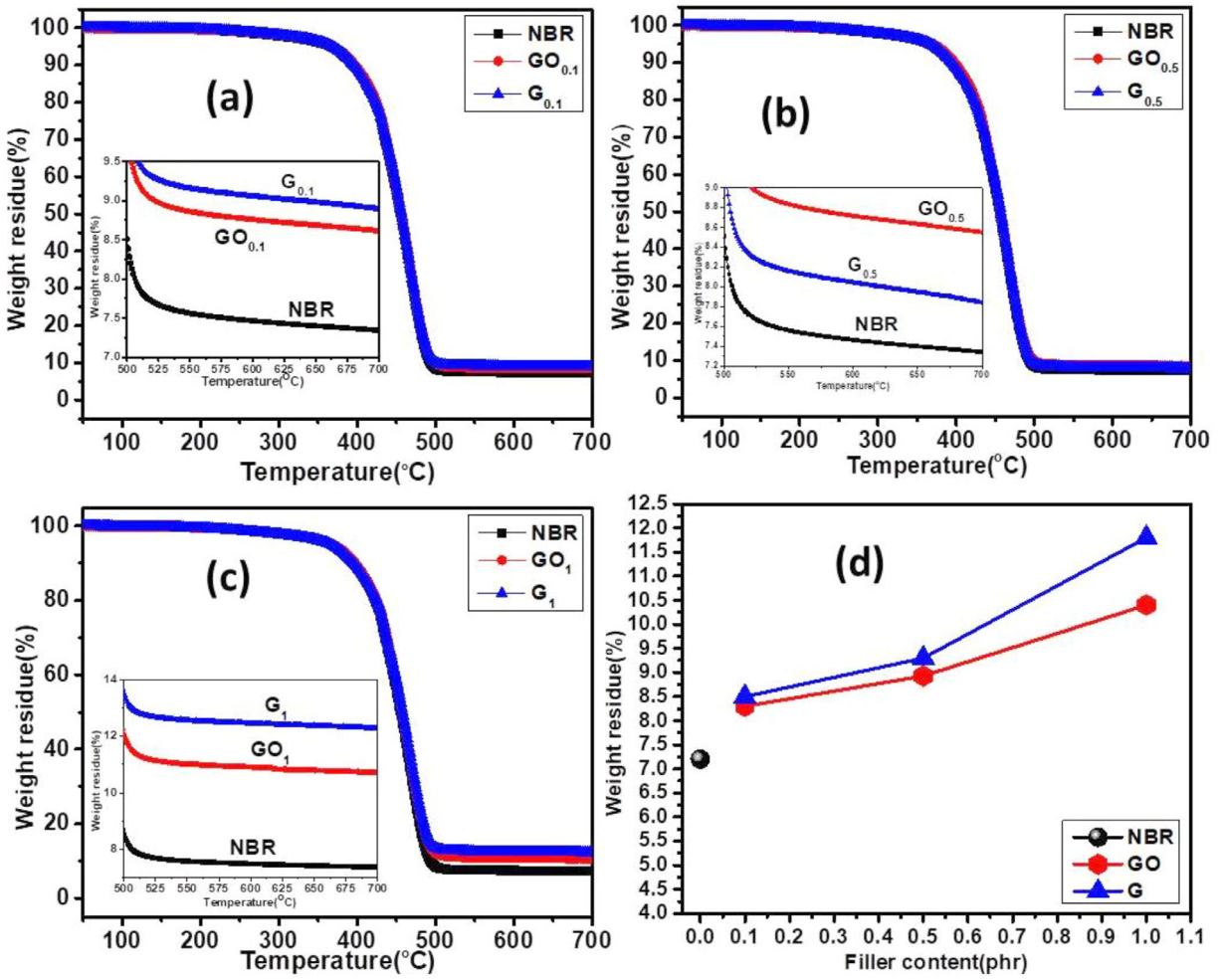

Fig. 9. TGA curves depicting the effects of GO/G-sheets loading (0.1-1 phr of GO/G) on thermal degradation of NBR in nitrogen medium (a, b and c) and (d) shows the effect of GO/G-sheets loading on the weight residues, Wr(%) of NBR.

reasons for the thermal degradation resistance of the composites, measured by W_r(%). As a result, pyrolysis products in GO/G-composites were delayed, causing further degradation of the primary matrix. Notably, the NBR-G composites outperformed NBR-GO composites in terms of W_r(%), even though NBR-GO showed higher T_{max} (°C) characteristics than NBR-G, particularly at lower loading levels (0.1∼0.5 phr).

The oxidation of graphite leads to wrinkled/corrugated GO sheets with reduction of the π-π interactions. Chemical reduction of GO with hydrazine in the presence of ammonia hydroxide, restores the sheet-like structures and the π-π interactions [26,49,50]. The restored structure of G, the π-π interaction and the phenyl groups together enhanced the thermal stability of the NBR matrix [26,46] compared to the highly distorted GO sheets. According to Chu et al. [65], a more wrinkled graphene sheets will exhibit lower thermal conductivity, since the wavy nature of the sheets significantly affects the intrinsic characteristics like the aspect ratio of the sheets. Thus, G-sheets may exhibit higher thermal conductivity with corresponding high thermal degradation stability compared to GO-sheets [71,84,85] when blended with NBR matrix. This may be a contributing factor for the high W_r(%) observed for NBR-G sheets. The higher thermal conductivity behavior of the G-sheets, might have resulted in the reduction of the photon scattering or acoustic impedance mismatch regions at the interface between NBR and G-sheets [41]. On the other hand, NBR-GO compounds recorded higher T_{max} (°C) because of strong bonds; NBR−S_x−GO−S−NBR or O−$H^{\sigma+}$−N $^{\sigma-}$−C− that needed to be broken in the course of the thermal process before the decompositions process comes to completion. The thermal breakdown of the oxygen moieties on GO into functionalities might have increased the pyrolysis of the NBR leading to high weight loss (%) of the NBR-GO. At 1 phr, T_{max} (°C) for GO_1 seems to be decreasing; this may be due to agglomeration tendency of GO sheets within NBR, similar to what was observed earlier by Mensah et al.[32,36,50]. In nitrogen medium, the thermal degradation resistances measured by T_{max} and W_r(%) for the current compositions showed significant improvement compared to those earlier reported for rubber reinforced with higher content, functionalized or formation of hybrid system with GDS, as compared in Table 2 with their remarks.

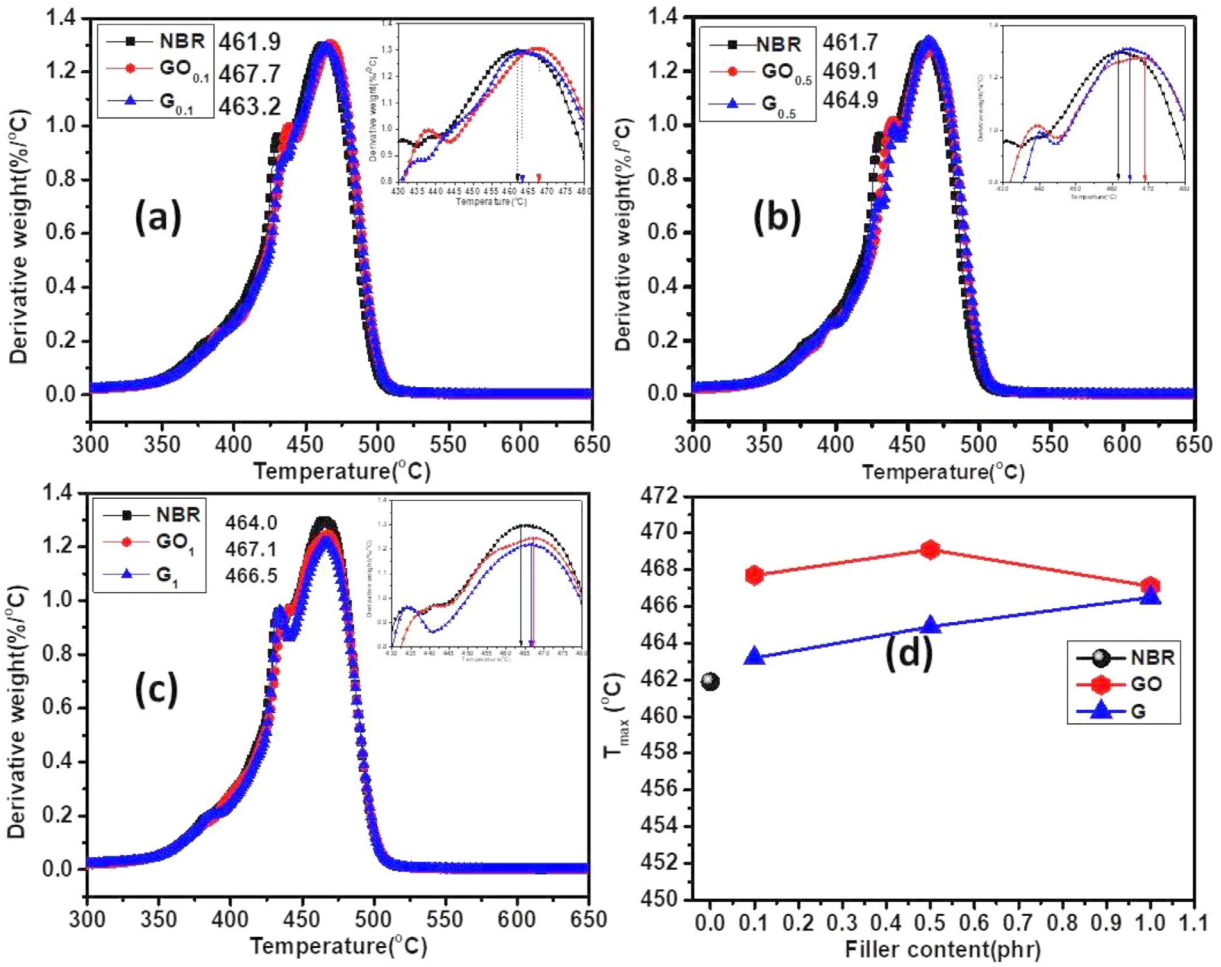

Fig. 10. DTG curves of NBR, filled different mounts of GO/G-sheets in nitrogen medium; (a) NBR, filled with 0.1 phr of GO/G (b), NBR filled with 0.5 phr of GO/G-sheets, (c) 1 phr filled with GO/G-sheets and (d) effect of GO/G-sheets on Tmax (°C) for the various compositions.

Table 1
Compositional formulation of NBR, GO and G compounds (unit phr).

Code	NBR	ZnO	CZ	SA	TMTD	S	GO/G
NBR	100	5	0.5	1.5	0.25	2	0
$GO_{0.1}$	100	5	0.5	1.5	0.25	2	0.1
$GO_{0.5}$	100	5	0.5	1.5	0.25	2	0.5
GO_1	100	5	0.5	1.5	0.25	2	1
$G_{0.1}$	100	5	0.5	1.5	0.25	2	0.1
$G_{0.5}$	100	5	0.5	1.5	0.25	2	0.5
G_1	100	5	0.5	1.5	0.25	2	1

phr: parts per hundred of rubber; CZ, N-cyclohexyl-2-benzothiazolysulfenamide; TMTD, tetramethylthiuram disulfide S; sulfur, SA; stearic acid.

Thermal degradation of NBR-GO/G in oxygen medium

The TGA plot for weight residue, W_r(%) versus temperature, for the NBR filled with different content (0.1∼1 phr) of GO and G, decomposed in oxidative medium are presented in Fig. 11 (*a* & *b)* with magnified graphs inserted in each plots for clarity. The effect of GO or G content on the W_r(%) are also compared in Fig. 11c. Regardless of the physical presence of the GO or G sheets, the content in the matrix or their interactions with the NBR matrix, it was fascinating to observe that the virgin NBR exhibited tremendous increase in W_r(%) than the composites. For instance, NBR showed ∼89, ∼21 and ∼86 % than $G_{0.1}$, $G_{0.5}$ and G_1 respectively and ∼154, ∼350, ∼92 % higher than the respective $GO_{0.1}$, $GO_{0.5}$ and GO_1 samples. Parallel to the case of Nitrogen medium, the NBR-G composites generally showed better W_r(%) than the NBR-GO in the oxygen medium, seen in Fig. 11c.

Table 2
Comparing T_{max} (°C) and weight residue W_r(%) of current samples and those reported.

Composition/code	% increase in W_r (%)	T_{max}(°C)	Remarks
NBR	~7.2	~469	Current work
$GO_{0.1}$ (0.1 phr GO)	~8.3/7.2 (~15 % > NBR)	~468	-
$GO_{0.5}$(0.5 phr GO)	~8.9/7.2 (~24 % > NBR)	~469	-
GO_1 (1 phr GO)	~10.4/7.2(~29 % > NBR)	~467	-
G0.1 (0.1 phr G)	~8.5/7.2(~18 '% > NBR)	~463	-
$G_{0.5}$ (0.5 phr G)	~9.3/7.2(~29 % > NBR)	~465	-
G_1 (1 phr G)	~11.8/7.2(~64 % > NBR)	~467	-
BIIR[a] (4wt% GO-IL)	-	~405	2013 [41]
NBR (1 phr GO)[b]	~9.4/7.8 (21% > NBR)		2014 [46]
SBR (7 phr G)	~10/6 (67% > SBR)	-	2014 [86]
XNBR (2 phr GO-HDA)[c]	~6.5/4 (63% > XNBR)	-	2017 [42]
NR (1.1 phr of G)	~12/8 (50% > NR)	~460	2020 [25]
PUR (1.9 phr PEG-MGO)[d]	~1.2/1(20% > PUR)	~475	2022 [87]
SBR(1.5 wt% GO)[e]	~5.1/2.2(132% > SBR)	~321	2022 [88]
SBR(2.5 wt% GO)[f]	~4.8/2.2(182% > SBR)	~319	2022 [88]
SR (1 wt% G-BN)[g]	~22.5/14.5(55% > SR)	-	2022 [89]

[a] GO functionalized ionic liquid in bromo-isoprene isobutylene rubber (BIIR).
[b] NBR: author's previous work, and
[c,d] GO functionalized with hexadecyl amine (HDA), Polyurthned rubber (PUR) reinforced with Polyethylene glycol (PEG, molecular weight 600) functionalized multilayer graphene oxide (MGO).
[e,f] GO functionalized with elastin collagen (COL),
[g] silicone rubber(SR) reinforced with (1:1) ratio of Multilayer graphenes (MG) and boron nitride (BN) nanosheets.

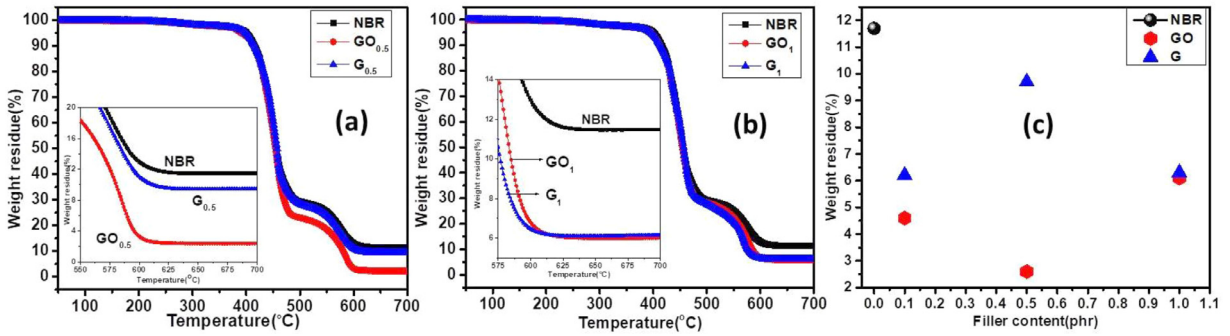

Fig. 11. TGA curves showing the effects of GO/G-sheets loading on thermal degradation of NBR in oxygen medium; (a) NBR filled with 0.5 phr GO/G-sheets (b) NBR filled with 1 phr GO/G-sheets and (c) the effect of GO/G-sheets loading on the Wr(%) of NBR.

The derivative thermographs (DTG) of the compounds decomposed in O_2(g) medium are shown in Fig. 12 (a-d). About three major degradations can be observed similar to those recently reported for BIIR by Zang et al. [44]. The first, second and third stages of degradation include; ~377-398 °C, ~451-457.2 °C and ~572.8-580.5 °C respectively. The initial stage of decomposition (shown as small neck on the DTG curves) may be due to burning of very weak bonds/structures in GO/G sheets. It is interesting to observe that the pure NBR matrix did not show such peaks. However, oxidation and rupture of side groups in silicone rubber chains was observed at ~365 °C by Wang et al. [35], on burning in O_2(g) medium. This is an indication of thermal degradation stability of polar NBR than silicone matrix. The pyrolysis or de-polymerization of the main NBR matrix occurred during the second stage of decomposition (~451-457.2 °C) where T_{max} (°C) occurs. Even so, the nanocomposites generally exhibited higher T_{max} (°C) temperature at this decompositions due to the presence of GO/G-sheets as barrier fillers and strong filler-NBR bonds [35]. As seen in Fig. 12d. here the G-sheets showed higher T_{max} (°C), which suggests it contributed to the delay of oxygen entering into the matrix to cause thermal oxidation/pyrolysis in NBR-G than the case of the highly wrinkled counterpart (GO-sheets) coated with high content of thermal oxidation accelerators(Oxygen groups). The third decomposition stage which appeared at the right-neck of the DTG curve around ~572.8-580.5 °C may be due to combustion of the matrix into ashes, associated with high weight residue W_r(%) and low weight loss (%) for the pure matrix compared with the nanocomposites.

The poor thermal degradation stability behavior of the NBR-GO/G nanocomposites in this medium may be due to thermo-oxidative decomposition of the backbone of NBR accelerated by the highly oxygenated functionalities (C—O—C, —O—C=O and O—H) decorating GO/G sheets [26,28], According to Zang et al. [44], oligomers are formed during thermal chain scission of BIIR in the presence of oxygen. A large amount of hydrocarbon gas is generated, associated with a severe weight loss. This is similar to the case observed for the NBR-GO/G composites of this present study.

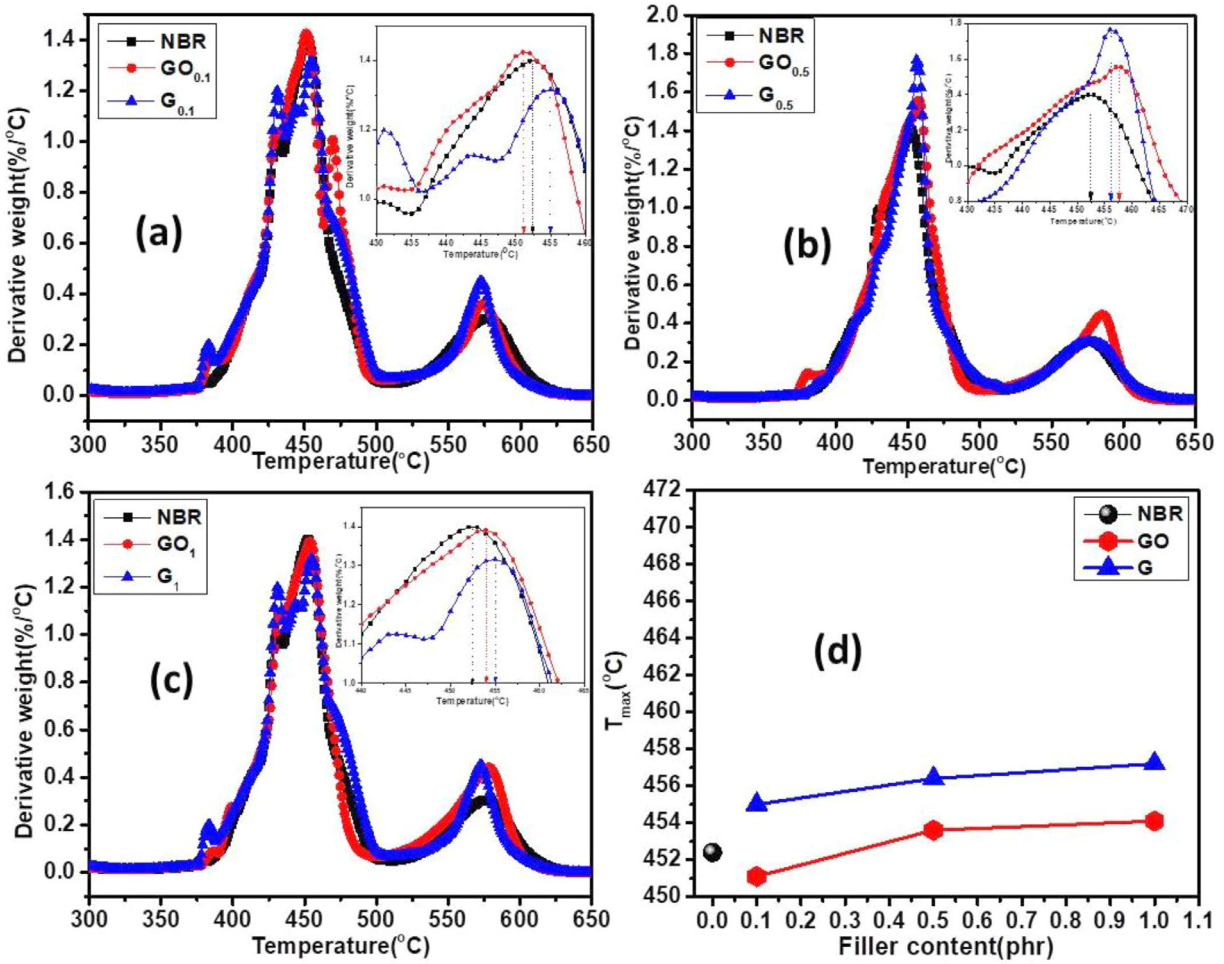

Fig. 12. DTG curves of NBR, filled different mounts of GO/G-sheets in oxygen medium; (a) NBR, filled with 0.1 phr of GO/G (b), NBR filled with 0.5 phr of GO/G-sheets, (c) 1 phr filled with GO/G-sheets and (d) effect of GO/G-sheets on Tmax (°C) for the various compositions.

Initial, final and procedural degradation temperature

The initial IDT (°C) and final FDT (°C) degradation temperatures of NBR, NBR-GO/G compounds during decomposition in N_2(g) and O_2(g) media are respectively presented in Fig. 13a and Fig. 13b. Also, the integral procedural degradation temperatures, IPDT (°C), which represents the volatile part of the compounds during decomposition in N_2(g) and O_2(g) media are also compared in Fig. 13c and Fig. 13d respectively. In N_2(g), the G-composites seem to show relatively higher IDT(°C) than the remaining compounds. However, all the samples maintained similar levels of FDT (°C) as seen in Fig. 13a. A similar observation was made in the O_2(g) medium, except that FDT(°C) of the compositions was higher than in N_2(g) medium. In Fig. 13c, the nanocomposites showed higher IPDT (°C) than the pure NBR, owing to the barrier effect provided by the GO and G-sheets in the matrix which slowed down degradation of the bulk matrix. On other hand, the pure NBR showed higher IPDT (°C) than the composites in the O_2(g) medium in Fig. 13d. These results are consistent with the T_{max} (°C) and the weight residue (%) discussed earlier. Therefore, in the N_2(g) medium the GO/G altered the structure of NBR, thereby producing higher amount of char residue (%) which thermally insulated NBR and prevented or delayed the diffusion of oxygen and other volatile decomposition products from entering the nanocomposite structure [90]. The higher IPDT (°C) for the pure NBR than the composites was as result of the degradation process which was facilitated by the thermal oxidation promoters (C—O—C, —O—C=O and O—H) associated with GO and G fillers.

Activation energy of thermal decomposition

According to Zhang et al. [44], temperature has an indirect association with molecular chain movement, chain relaxation, and decomposition activation energy. To understand the overall thermal degradation behavior of the compounds, an investigation of the decomposition kinetics of NBR and NBR-GO/G composites was required. The activation energy E_a(KJ/mol) for thermal decompositions in both in N_2(g) and O_2(g) media of the various composition was obtained by the plots of ln $[\ln(1\text{-}\alpha)^{-1}]$ against $\Theta(T\text{-}T_{max})$ shown in Fig. 14a and Fig. 14b respectively for representative samples (NBR, GO_1 and G_1).

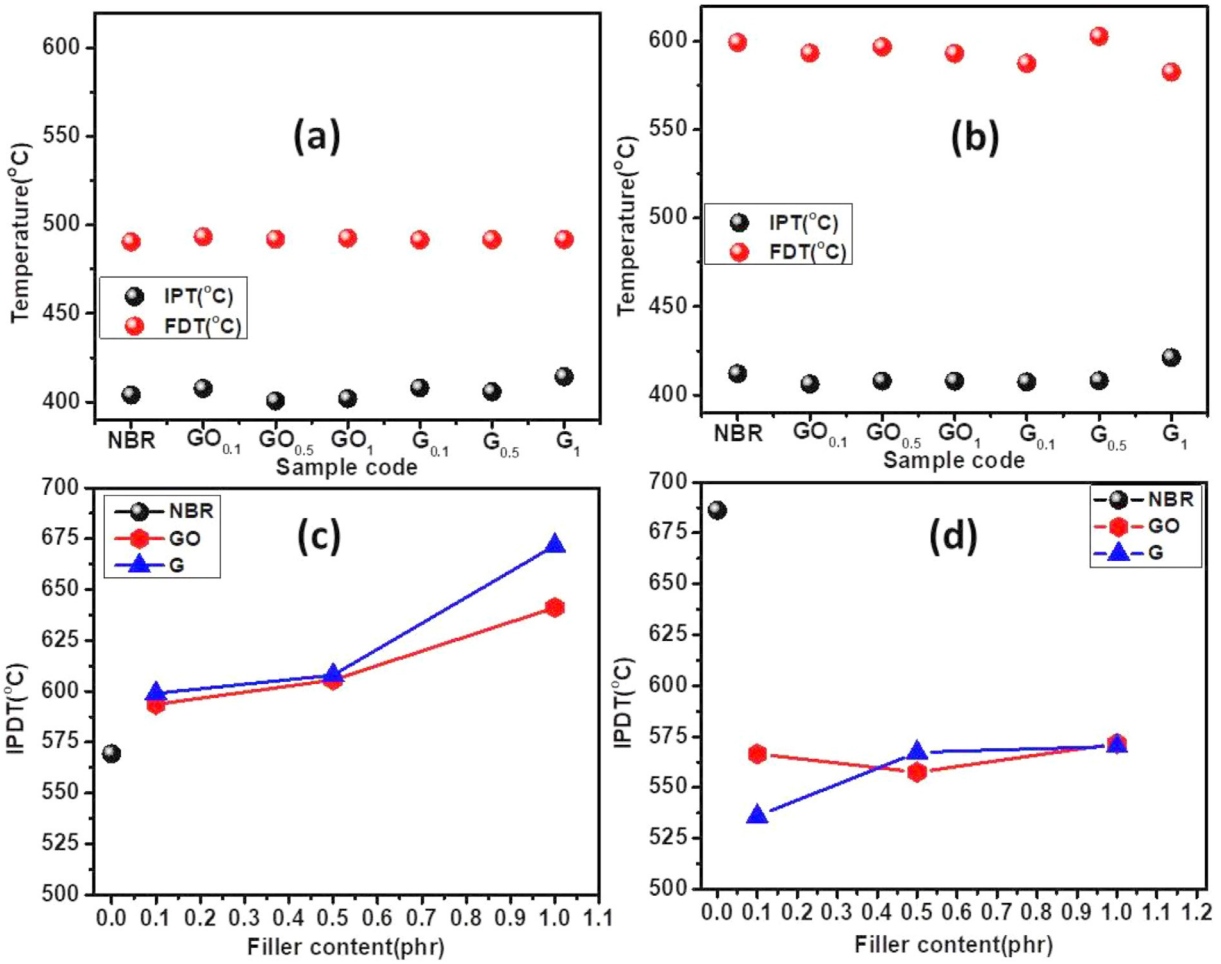

Fig. 13. The initial (IDT) and final (FDT) degradation temperatures of compounds in (a) N2(g) medium(b) O2(g) medium. The integral procedural degradation temperatures (IPDT) of the compounds in (c) N2(g) medium and (d) O2(g) medium.

The estimated E_a(KJ/mol) of the samples are compared in Fig. 14c and Fig. 14d respectively for N_2(g) and O_2(g) media. It was fascinating to observed that higher E_a(KJ/mol) was required for thermal breakdown of the NBR-GO in comparison with that of NBR-G composites and the gum in the N_2(g) medium. This was in correspondence with the high T_{max} (°C) observed for NBR-GO composites. In the O_2(g) medium, higher E_a(KJ/mol) was required to decompose the main chain of NBR as compared to the composites, this matched well with the corresponding W_r(%) recorded. Yet in the O_2(g) medium, higher E_a(KJ/mol) was needed to decompose NBR-GO composites, associated with relatively higher weight loss (%) as compared with the NBR-G composites. Generally, E_a(KJ/mol) is influenced by nature of reactants and the presence of a catalyst. Herein, the tight bonding in NBR-GO: NBR—S_x—GO—S—NBR and NBR—O—$H^{\sigma+}$—$N^{\sigma-}$—C—NBR caused by the active oxygen groups (C—O—C, —O—C=O and O—H) on GO may have raised the E_a(KJ/mol) for decomposition, even though the final products led to lower W_r(%).In addition, further crosslinking reactions have been observed in elastomers like BIIR and polychloroprene rubber (CR) during the thermal degradation process, owing to the recombination of the radical fragments produced [41]. This phenomenon is likely to further increase the E_a(KJ/mol) for decomposing of NBR-GO composites in both N_2(g) and O_2(g) media compared to NBR-G composites.

While thermo-oxidative induced crosslinking density may also be possible in the nitrogen medium (Fig. 14c) for the composites, especially for NBR-GO, it was not consistent in the case of O_2(g) medium, as the composites decomposed severely with relatively lower E_a(KJ/mol) and W_r(%) relative to that of the pure matrix. It is interesting to observe that NBR-G exhibited lower E_a(KJ/mol) for decomposition in both N_2(g) and O_2(g) media (obviously at lower filler content: 0.1-0.5 phr G), although the final W_r(%) in both media were the best. This may be due to the presence of the residual hydrazine (N_2H_4) present within the structures of G-sheets which acted as catalyst by lowering the E_a(KJ/mol) barrier for the decomposition of the G-sheets in the bulk NBR-G composites. This is evident in the N_2 (g) medium (Fig. 14c) than in O_2(g) medium (Fig. 14d), despite the lower weight loss (%) observed for the final products. This observation is in accordance with the earlier work on N_2H_4 reported by dos Santos et al. [91] which investigated the thermal decomposition of N_2H_4 using TGA. It was

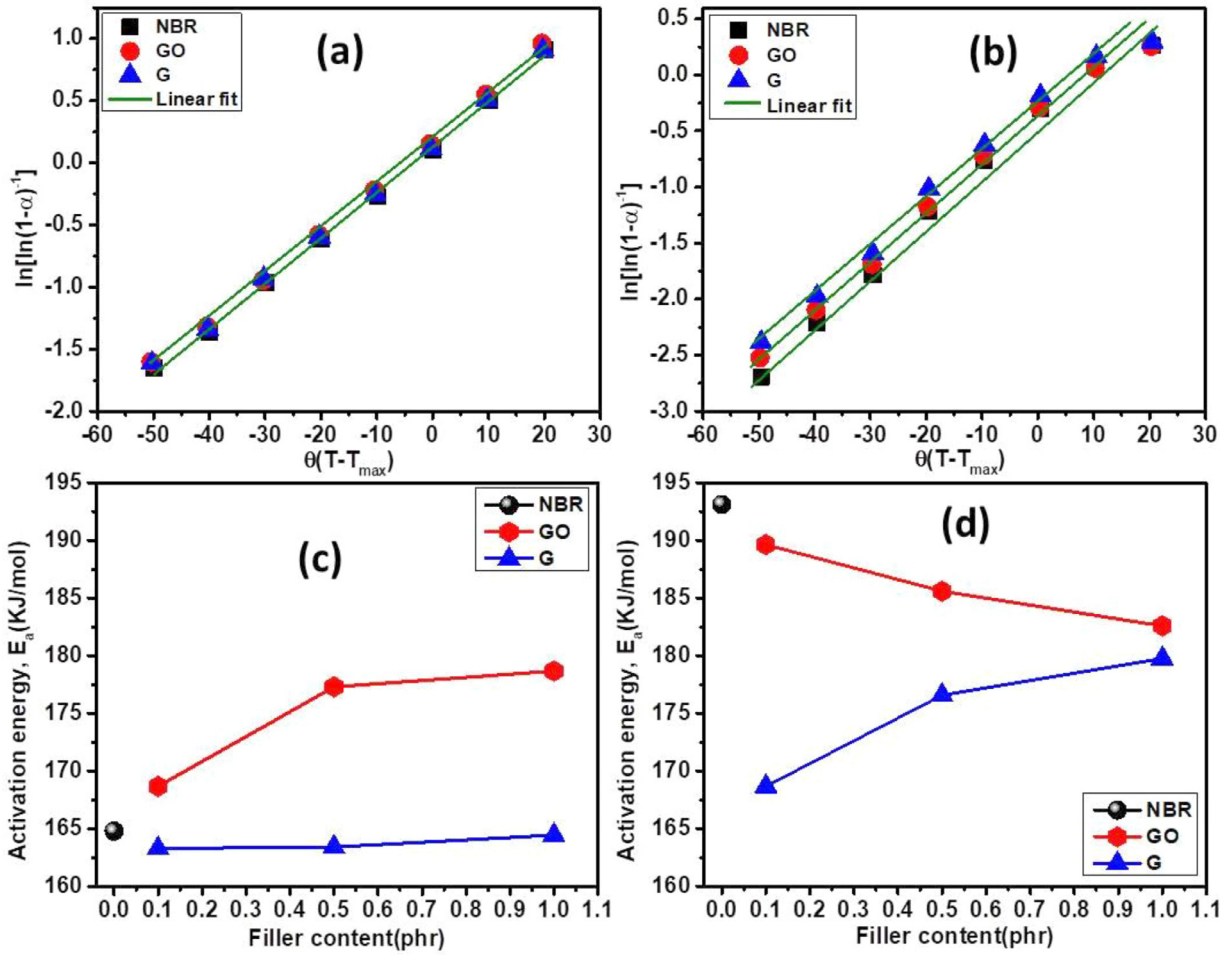

Fig. 14. The plots of ln [ln(1-α)−1] against Θ(T-Tmax) for the NBR, GO1 and G1 in (a) nitrogen medium(b) air medium and (c) effect of GO/G-sheet loading on activation energy in nitrogen medium (d) effect of GO/G-sheet loading on activation energy in oxygen medium.

concluded that N_2H_4 is thermodynamically unstable, which is subject to spontaneous decomposition reactions, even at ambient temperature, and it is more reactive in nitrogen atmosphere than in oxygen one. Hence, the thermal instability nature of N_2H_4 traces in G-sheets could have sped up the burning process of NBR-G composites, associated with lower E_a(KJ/mol).

Conclusion

The preparation of acrylonitrile-butadiene rubber (NBR) reinforced with graphene oxide (GO) and reduced graphene Oxide (G) nanocomposites were achieved by the combination of solution and open-roll blending techniques. The curing behavior, dispersions of GO/G-sheets in NBR, crosslinking density and compression sets, CS (%), were investigated. Also, the thermal degradation behavior of the NBR-GO/G composites was separately investigated in air O_2(g) and nitrogen N_2(g) media at 800°C, using Thermal gravimetric Analysis (TGA). Solution mixing technique was very efficient as the NBR-GO/G composites exhibited higher network density, rheological strengths (M_H and ΔM) and high CS (%) than NBR. Also, the char yield of the composites was observed to be high, as its delayed further degradation of the NBR matrix in N_2(g) medium, with lower amounts of weight loss (%), higher maximum degradation temperatures (IPDT and T_{max})/(°C) and higher amounts of activation energy E_a (KJ/mol) for decomposition, particularly for the NBR-GO composites. This was due to the presence of the GO/G-sheets and their strong bond with the NBR matrix. In the O_2(g) medium, severe degradation of NBR matrix occurred, irrespective of the content of GO/G-sheets incorporated. Thus, in the O_2(g) medium, insignificant char yield was available to protect the backbone of NBR matrix from thermal scission, as degradation was accelerated by the highly oxygenated groups (C–O–C, –O–C=O and O–H)) on the GO/G-sheets. The harsh decomposition of the composite was associated with large amount of weight loss (%) and relatively lower activation energy, E_a (KJ/mol) of decomposition as compared to NBR. When compared, NBR-G sheet exhibited higher weight residue, W_r (%) compared to NBR-GO composites in all decomposition media. In the N_2(g) medium, NBR-GO composites exhibited high T_{max} (°C) than NBR-G composites, due to the tight

structures induced by the oxygenated moieties. The NBR-G on the other hand, showed higher W_r (%) than NBR-GO composites suspected to be due to the high thermal conductivity property of less wrinkled G-sheets, as compared to the highly wrinkled GO-sheets. In terms of kinetics of decomposition, NBR-GO composites generally slowed down of NBR than NBR-G composites. This was suspected to be due to the presence of strong bonds like NBR—S_x—GO—S—NBR and NBR—O—$H^{\sigma+}$—N $^{\sigma-}$—C—NBR which raised the E_a (KJ/mol) for decomposition. The number of these bonds may be lower in the case of NBR-G, due to the lower Oxygen-Carbon ratio of G-sheets as compared to GO-sheets. Therefore, in the use of GDS fillers in rubber matrix for high-temperature applications, the nature of GDS, the matrix and the environment of use, must be considered in the design to achieve optimal results. Finally, these NBR-GO/G composites can be used for high temperature and pressure applications including oil and gas seals, gaskets materials and rubber products for oil and gas drilling hoses after careful optimization.

Data availability statement

The data used to support the findings of this study are available from the corresponding author upon request.

Funding statement

There was no funding for this research work (self-funding)

Declaration of Competing Interest

The authors declare no competing financial interest.

Acknowledgement

We acknowledge the support from Professor Changwoon Nah (Intelligent Polymer Nano-materials Lab) of Polymer Nanoscience and Technology Department, Jeonbuk National University (South Korea), for allowing us to use their facility to carry out this study. We also acknowledge the University of Ghana – Carnegie Next Generation of African Academics (UG-Carnegie NGAA) Project and the Office of Research Innovation and Development (ORID) at the University of Ghana for their guidance towards the completion of the manuscript.

References

[1] C.S. Boland, U. Khan, C. Backes, A. O'Neill, J. McCauley, S. Duane, R. Shanker, Y. Liu, I. Jurewicz, A.B. Dalton, J.N. Coleman, Sensitive, high-strain, high-rate bodily motion sensors based on graphene-rubber composites, ACS Nano 8 (2014) 8819–8830.
[2] I. Kang, M.J. Schulz, J.H. Kim, V. Shanov, D. Shi, A carbon nanotube strain sensor for structural health monitoring, Smart mater. structures 15 (2006) 737.
[3] O. Kanoun, C. Mueller, A. Benchirouf, A. Sanli, D. Trong Nghia, A. Al-Hamry, L. Bu, C. Gerlach, A. Bouhamed, Flexible carbon nanotube films for high performance strain sensors, Sensors 14 (2014) 10042–10071.
[4] J.R. Garcia, D. O'Suilleabhain, H. Kaur, J.N. Coleman, A simple model relating gauge factor to filler loading in nanocomposite strain sensors, ACS Appl. Nano Ma.s 4 (2021) 2876–2886.
[5] L. Huang, H. Wang, P. Wu, W. Huang, W. Gao, F. Fang, N. Cai, R. Chen, Z. Zhu, wearable flexible strain sensor based on three-dimensional wavy laser-induced graphene and silicone rubber, Sensors 20 (2020) 4266.
[6] H.R. Na, H.J. Lee, J.H. Jeon, H.-J. Kim, S.-K. Jerng, S.B. Roy, S.-H. Chun, S. Lee, Y.J. Yun, Vertical graphene on flexible substrate, overcoming limits of crack-based resistive strain sensors, npj Flexible Electronics 6 (2022) 2.
[7] J. Abd Razak, Graphene Nanoplatelets-Filled NR/EPDM Rubber Blend: Effects of GNPs Loading on Blend Processability, Mechanical Properties and Fracture Morphology, Nova Science Publishers, Inc, 2015.
[8] S. Chandran C, S. Yaragalla, N. Kalarikkal, R. Subban, C.H. Chan, S. Thomas, Effect of reinforcement on the barrier and dielectric properties of epoxidized natural rubber–graphene nanocomposites, POLYMER ENG. SCI. 55 (2015).
[9] H.N. Azlina, H.A. Sahrim, R. Rozaidi, Enhanced Tensile and Dynamic Mechanical Properties of Thermoplastic Natural Rubber Nanocomposites, Polymer–Plastics Technol. En. 50 (2011) 1383–1387.
[10] Z.-H. Chang, F. Guo, J.-F. Chen, J.-H. Yu, G.-Q. Wang, Synergistic flame retardant effects of nano-kaolin and nano-HAO on LDPE/EPDM composites, Polymer Degradation and Stability 92 (2007) 1204–1212.
[11] Z. Wu, H. Wang, X. Tian, X. Ding, M. Xue, H. Zhou, K. Zheng, Mechanical and flame-retardant properties of styrene–ethylene–butylene–styrene/carbon nanotube composites containing bisphenol A bis(diphenyl phosphate), Composites Sci. Technol. 82 (2013) 8–14.
[12] M. Balachandran, S.S. Bhagawan, Mechanical, thermal, and transport properties of nitrile rubber-nanocalcium carbonate composites, J. Appl. Polymer Science 126 (2012) 1983–1992.
[13] S. Botros, M. Tawfic, Compatibility and thermal stability of EPDM-NBR elastomer blends, J. Elastomers & Plastics 37 (2005) 299–317.
[14] T.D. Dao, H.I. Lee, H.M. Jeong, Alumina-coated graphene nanosheet and its composite of acrylic rubber, J. colloid and interface sci. 416 (2014) 38–43.
[15] A. Das, D.-Y. Wang, K.W. Stöckelhuber, R. Jurk, J. Fritzsche, M. Klüppel, G. Heinrich, Rubber–clay nanocomposites: some recent results, Adv. Rubber Composites (2010) 85–166.
[16] M.A. López-Manchado, M. Arroyo, B. Herrero, J. Biagiotti, Vulcanization kinetics of natural rubber–organoclay nanocomposites, J. Appl. Polymer Sci. 89 (2003) 1–15.
[17] M. Maiti, A.K. Bhowmick, Effect of polymer–clay interaction on solvent transport behavior of fluoroelastomer–clay nanocomposites and prediction of aspect ratio of nanoclay, J. App. Polymer Sci. 105 (2007) 435–445.
[18] B. Mensah, H.G. Kim, J.-H. Lee, S. Arepalli, C. Nah, Carbon nanotube-reinforced elastomeric nanocomposites: a review, Int. J. Smart and Nano Mater. 6 (2015) 211–238.
[19] M. Norkhairunnisa, A. Azizan, M. Mariatti, H. Ismail, L. Sim, Thermal stability and electrical behavior of polydimethylsiloxane nanocomposites with carbon nanotubes and carbon black fillers, J. Composite Mater. 46 (2011) 903–910.

[20] Y. Zhang, Y. Fan, U. Kamran, S.-J. Park, Improved thermal conductivity and mechanical property of mercapto group-activated boron nitride/elastomer composites for thermal management, Composites Part A: Appl. Sci. Manufacturing 156 (2022) 106869.
[21] S.-S. Choi, Effect of bound rubber on characteristics of highly filled styrene–butadiene rubber compounds with different types of carbon black, J. Appl. Polymer Sci. 93 (2004) 1001–1006.
[22] F.G. Souza, M.E. Sena, B.G. Soares, Thermally stable conducting composites based on a carbon black-filled polyoxadiazole matrix, J. App. Polymer Sci. 93 (2004) 1631–1637.
[23] C.-L. Chiang, R.-C. Chang, Y.-C. Chiu, Thermal stability and degradation kinetics of novel organic/inorganic epoxy hybrid containing nitrogen/silicon/phosphorus by sol-gel method, Thermochimica Acta 453 (2007) 97–104.
[24] C.N. Bismark Mensah, Reinforcing Acrylonitrile Rubber with Graphene: Inspection of Mechanical, Thermal and Cure Kinetics Properties, Nanotech La Defense, Paris, France (2016).
[25] Z. Dong, F. Cai, Z. Jiang, W. Xu, Thermal Property Studies of In Situ Blended Graphene/Nature Rubber Nanocomposites, Int. J. Polymer Sci. 2020 (2020) 4694213.
[26] B. Mensah, K.C. Gupta, H. Kim, W. Wang, K.-U. Jeong, C. Nah, Graphene-reinforced elastomeric nanocomposites: A review, Polym. Test 68 (2018) 160–184.
[27] E. George, J. Joy, S. Anas, Acrylonitrile-based polymer/graphene nanocomposites: A review, Polymer Composites 42 (2021) 4961–4980.
[28] H. Zhang, W. Xing, H. Li, Z. Xie, G. Huang, J. Wu, Fundamental researches on graphene/rubber nanocomposites, Adv. Industrial Eng. Polymer Res. 2 (2019) 32–41.
[29] K.S. Novoselov, A.K. Geim, S.V. Morozov, D. Jiang, Y. Zhang, S.V. Dubonos, I.V. Grigorieva, A.A. Firsov, Electric field effect in atomically thin carbon films, Science 306 (2004) 666–669.
[30] A.K. Geim, Graphene: status and prospects, Science 324 (2009) 1530–1534.
[31] X. Bai, C. Wan, Y. Zhang, Y. Zhai, Reinforcement of hydrogenated carboxylated nitrile–butadiene rubber with exfoliated graphene oxide, Carbon 49 (2011) 1608–1613.
[32] B. Mensah, K.C. Gupta, G. Kang, H. Lee, C. Nah, A comparative study on vulcanization behavior of acrylonitrile-butadiene rubber reinforced with graphene oxide and reduced graphene oxide as fillers, Polym. Test 76 (2019) 127–137.
[33] J. Wu, W. Xing, G. Huang, H. Li, M. Tang, S. Wu, Y. Liu, Vulcanization kinetics of graphene/natural rubber nanocomposites, Polymer 54 (2013) 3314–3323.
[34] P. Marlina, H. Prasetya, A. Nugroho, M. Yusya, R. Andika, S. Haryati, The rheological and mechanical properties of natural rubber/graphene composites, IOP Conference Series: Earth and Environmental Science, IOP Publishing, 2022.
[35] Y. Wang, X. Qiu, J. Zheng, Effect of the sheet size on the thermal stability of silicone rubber–reduced graphene oxide nanocomposites, J. App. Polymer Sci. 136 (2019) 47034.
[36] B. Mensah, S.I. Kang, W. Wang, C. Nah, Effect of graphene on polar and nonpolar rubber matrices, Mechan. Adv. Materia. Modern Processes 4 (2018) 1.
[37] N. Yan, G. Buonocore, M. Lavorgna, S. Kaciulis, S.K. Balijepalli, Y. Zhan, H. Xia, L. Ambrosio, The role of reduced graphene oxide on chemical, mechanical and barrier properties of natural rubber composites, Composites Sci. Technol. 102 (2014) 74–81.
[38] S. Yaragalla, C.S. Chandran, N. Kalarikkal, R. Subban, C.H. Chan, S. Thomas, Effect of reinforcement on the barrier and dielectric properties of epoxidized natural rubber–graphene nanocomposites, Polymer Eng. Sci. 55 (2015) 2439–2447.
[39] H. Qin, C. Deng, S. Lu, Y. Yang, G. Guan, Z. Liu, Q. Yu, Enhanced mechanical property, thermal and electrical conductivity of natural rubber/graphene nanosheets nanocomposites, Polymer Composites 41 (2020) 1299–1309.
[40] J. Wilk, R. Smusz, R. Filip, G. Chmiel, T. Bednarczyk, Experimental investigations on graphene oxide/rubber composite thermal conductivity, Scientific rep. 10 (2020) 15533.
[41] X. Xiong, J. Wang, H. Jia, E. Fang, L. Ding, Structure, thermal conductivity, and thermal stability of bromobutyl rubber nanocomposites with ionic liquid modified graphene oxide, Polymer degradation and stability 98 (2013) 2208–2214.
[42] R. Manna, S.K. Srivastava, Fabrication of functionalized graphene filled carboxylated nitrile rubber nanocomposites as flexible dielectric materials, Mater. Chem. Front. 1 (2017) 780–788.
[43] T. Ozawa, A new method of analyzing thermogravimetric data, Bull. chem. society Jpn 38 (1965) 1881–1886.
[44] W. Zhang, Y. Zang, Y. Lu, W. Lin, S. Zhao, J. Xiong, Thermal Decomposition of Brominated Butyl Rubber (2021) 14.
[45] H.E. Kissinger, Reaction kinetics in differential thermal analysis, Analytical chem. 29 (1957) 1702–1706.
[46] B. Mensah, S. Kim, S. Arepalli, C. Nah, A Study of Graphene Oxide-Reinforced Rubber Nanocomposite, J. App. Polymer Sci. 131 (2014).
[47] C.D. Doyle, ESTIMATING THERMAL STABILITY OF EXPERIMENTAL POLYMERS BY EMPIRICAL THERMOGRAVIMETRIC ANALYSIS, Analytical Chemi. 33 (1961) 77 -&.
[48] F.-L. Jin, S.-J. Park, Thermal properties of epoxy resin/filler hybrid composites, Polymer Degradation and Stability 97 (2012) 2148–2153.
[49] LEILA SHAHRIARY, A.A. ATHAWALE, Graphene Oxide Synthesized by using Modified Hummers Approach, Int. J. Renewable Energy and Environ. Eng. (2014) 02.
[50] B. Mensah, D. Kumar, D.K. Lim, S. Kim, B.H. Jeong, C. Nah, Preparation and properties of acrylonitrile–butadiene rubber–graphene nanocomposites, J. App. Polymer Sci. 132 (2015).
[51] B. Mensah, D. Kumar, D.-K. Lim, S.G. Kim, B.-H. Jeong, C. Nah, Preparation and properties of acrylonitrile–butadiene rubber–graphene nanocomposites, J. App. Polymer Sci. 132 (2015) n/a-n/a.
[52] P.J. Flory, J. Rehner, Statistical Mechanics of Cross-Linked Polymer Networks II. Swelling, The J. Chem. Phys. 11 (1943) 521–526.
[53] G.M. Bristow, W.F. Watson, Cohesive energy densities of polymers. Part 1.-Cohesive energy densities of rubbers by swelling measurements, Transactions of the Faraday Society 54 (1958) 1731–1741.
[54] S. GS, C. Park, Y. Huh, J. Jeon, C. Yun, J. Won, K.-U. Jeong, C. Nah, ENHANCING THE REVERSION RESISTANCE, CROSSLINKING DENSITY AND THERMO-MECHANICAL PROPERTIES OF ACCELERATED SULFUR CURED CHLOROBUTYL RUBBER USING 4,4′-BIS (MALEIMIDO) DIPHENYL METHANE, Rubber Chem. Technol. (2018).
[55] V. Singh, D. Joung, L. Zhai, S. Das, S.I. Khondaker, S. Seal, Graphene based materials: Past, present and future, Progress in Materials Sci. 56 (2011) 1178–1271.
[56] H. Kim, A.A. Abdala, C.W. Macosko, Graphene/Polymer Nanocomposites, Macromolecules 43 (2010) 6515–6530.
[57] R.J. Young, I.A. Kinloch, L. Gong, K.S. Novoselov, The mechanics of graphene nanocomposites: A review, Composites Sci. Technol. 72 (2012) 1459–1476.
[58] P. Blake, E.W. Hill, A.H. Castro Neto, K.S. Novoselov, D. Jiang, R. Yang, T.J. Booth, A.K. Geim, Making graphene visible, Appl. Phys. Lett. 91 (2007).
[59] W.S. Hummers, R.E. Offeman, PREPARATION OF GRAPHITIC OXIDE, J. Am. Cheml Society 80 (1958) 1339.
[60] B. Mensah, D.S. Konadu, B. Agyei-Tuffour, Effects of Graphene Oxide and Reduced Graphene Oxide on the Mechanical and Dielectric Properties of Acrylonitrile-Butadiene Rubber and Ethylene-Propylene-Diene-Monomer Blend, Int. J. Polymer Sci. 2022 (2022) 8038386.
[61] T. Kuilla, S. Bhadra, D. Yao, N.H. Kim, S. Bose, J.H. Lee, Recent advances in graphene based polymer composites, Progress in Polymer Science 35 (2010) 1350–1375.
[62] M. Hernández, M.d.M. Bernal, R. Verdejo, T.A. Ezquerra, M.A. López-Manchado, Overall performance of natural rubber/graphene nanocomposites, Composites Science and Technology 73 (2012) 40–46.
[63] X. Liu, L.-Y. Wang, L.-F. Zhao, H.-F. He, X.-Y. Shao, G.-B. Fang, Z.-G. Wan, R.-C. Zeng, Research Progress of Graphene-Based Rubber Nanocomposites, Polymer Composites (2016) n/a-n/a.
[64] X. Liu, D. Sun, L. Wang, B. Guo, Sodium Humate Functionalized Graphene and Its Unique Reinforcement Effects for Rubber, Industrial & Engineering Chemistry Research 52 (2013) 14592–14600.

[65] K. Chu, W.-s. Li, H. Dong, Role of graphene waviness on the thermal conductivity of graphene composites, App. Phy. A 111 (2013) 221–225.
[66] C.N.R. Rao, U. Maitra, H.S.S.R. Matte, in: Synthesis, Characterization, and Selected Properties of Graphene, Graphene, Wiley-VCH Verlag GmbH & Co. KGaA, 2012, pp. 1–47.
[67] R. Sengupta, M. Bhattacharya, S. Bandyopadhyay, A.K. Bhowmick, A review on the mechanical and electrical properties of graphite and modified graphite reinforced polymer composites, Progress in Polymer Sci. 36 (2011) 638–670.
[68] X. Wu, T. Lin, Z. Tang, B. Guo, G. Huang, Natural rubber/graphene oxide composites: Effect of sheet size on mechanical properties and strain-induced crystallization behavior, Express Polymer Lett. 9 (2015).
[69] M. Akiba, A.S. Hashim, Vulcanization and crosslinking in elastomers, Progress in Polymer Scie 22 (1997) 475–521.
[70] M. López-Manchado, M. Arroyo, B. Herrero, J. Biagiotti, Vulcanization kinetics of natural rubber–organoclay nanocomposites, J. App. Polymer Sci. 89 (2003) 1–15.
[71] A. Alofi, Thermal conductivity of graphene and graphite, Phys. Rev. B 87 (2013).
[72] M. van Duin, Chemistry of EPDM cross-linking, Kautschuk Gummi Kunststoffe 55 (2002) 150 -+.
[73] A. Allahbakhsh, S. Mazinani, M.R. Kalaee, F. Sharif, Cure kinetics and chemorheology of EPDM/graphene oxide nanocomposites, Thermochimica Acta 563 (2013) 22–32.
[74] M.J. Azizli, M. Mokhtary, H.A. Khonakdar, V. Goodarzi, Compatibilizer/graphene/carboxylated acrylonitrile butadiene rubber (XNBR)/ethylenepropylenediene monomer (EPDM) nanocomposites: Morphology, compatibility, rheology and mechanical properties, J. App. Polymer Sci. 137 (2020) app49331.
[75] C. Nah, J.Y. Lim, R. Sengupta, B.H. Cho, A.N. Gent, Slipping of carbon nanotubes in a rubber matrix, Polymer Int. 60 (2011) 42–44.
[76] C. Nah, J.Y. Lim, B.H. Cho, C.K. Hong, A.N. Gent, Reinforcing rubber with carbon nanotubes, J. App. Polymer Sci. (2010) n/a-n/a.
[77] M.A. Rafiee, J. Rafiee, I. Srivastava, Z. Wang, H. Song, Z.-Z. Yu, N. Koratkar, Fracture and Fatigue in Graphene Nanocomposites, Small 6 (2010) 179–183.
[78] S. Stankovich, D.A. Dikin, G.H.B. Dommett, K.M. Kohlhaas, E.J. Zimney, E.A. Stach, R.D. Piner, S.T. Nguyen, R.S. Ruoff, Graphene-based composite materials, Nature 442 (2006) 282–286.
[79] R.J. Pazur, J.G. Cormier, K. Korhan-Taymaz, THE EFFECT OF ACRYLONITRILE CONTENT ON THE THERMO-OXIDATIVE AGING OF NITRILE RUBBER, Rubber Chem. Technol. 87 (2014) 53–69.
[80] T.V. Varghese, H. Ajith Kumar, S. Anitha, S. Ratheesh, R.S. Rajeev, V. Lakshmana Rao, Reinforcement of acrylonitrile butadiene rubber using pristine few layer graphene and its hybrid fillers, Carbon 61 (2013) 476–486.
[81] L. Gonzalez, A. Rodriguez, J.L. Valentin, A. Marcos-Fernandez, P. Posadas, Conventional and efficient crosslinking of natural rubber - Effect of heterogeneities on the physical properties, Kgk-Kautschuk Gummi Kunststoffe 58 (2005) 638–643.
[82] K. Senthilvel, S. Vishvanathperumal, B. Prabu, L.John Baruch, Studies on the morphology, cure characteristics and mechanical properties of acrylonitrile butadiene rubber with hybrid filler (carbon black/silica) composite, Polymers and Polymer Composites 24 (2016) 473–480.
[83] H. Zhang, Y. Wei, Z. Kang, G. Zhao, Y. Liu, Influence of graphene oxide and multiwalled carbon nanotubes on the dynamic mechanical properties and heat buildup of natural rubber/carbon black composites, J. Elastomers & Plastics 50 (2018) 403–418.
[84] S. Araby, L. Zhang, H.-C. Kuan, J.-B. Dai, P. Majewski, J. Ma, A novel approach to electrically and thermally conductive elastomers using graphene, Polymer 54 (2013) 3663–3670.
[85] S. Araby, Q. Meng, L. Zhang, H. Kang, P. Majewski, Y. Tang, J. Ma, Electrically and thermally conductive elastomer/graphene nanocomposites by solution mixing, Polymer 55 (2014) 201–210.
[86] W. Xing, M. Tang, J. Wu, G. Huang, H. li, Z. Lei, X. Fu, H. Li, Multifunctional properties of graphene/rubber nanocomposites fabricated by a modified latex compounding method, Composites Sci. Technol. 99 (2014).
[87] W. Fu, L. Wang, Z. Huang, X. Huang, Z. Su, Y. Liang, Z. Gao, Q. Pan, Comparison of Effects of Different Sacrificial Hydrogen Bonds on Performance of Polyurethane/Graphene Oxide Membrane, Membranes 12 (2022) 517.
[88] A. Khan, L.K. Kian, M. Jawaid, A.A.P. Khan, M.M. Alotaibi, A.M. Asiri, H.M. Marwani, Preparation of Styrene-Butadiene Rubber (SBR) Composite Incorporated with Collagen-Functionalized Graphene Oxide for Green Tire Application, Gels 8 (2022) 161.
[89] B. Deng, Y. Shi, X. Zhang, W. Ma, H. Liu, C. Gong, Thermally Conductive and Electrically Insulated Silicone Rubber Composites Incorporated with Boron Nitride−Multilayer Graphene Hybrid Nanofiller, Nanomaterials 12 (2022) 2335.
[90] A. BOONMAHITTHISUD, S. CHUAYJULJIT, NR/XSBR Nanocomposites with Carbon Black and Carbon Nanotube Prepared by Latex Compounding, J. Metals, Materials and Minerals 22 (2012) 77–85.
[91] L. dos Santos, C. Ribeiro, J. Capela, M. Crespi, M. Pimentel, M. Julio, Kinetic parameters for thermal decomposition of hydrazine, J. Thermal Ana. Calorimetry 113 (2013).